

**HYBRID DOMAIN DECOMPOSITION ALGORITHMS FOR
COMPRESSIBLE AND ALMOST INCOMPRESSIBLE ELASTICITY
TR2008-919**

CLARK R. DOHRMANN* AND OLOF B. WIDLUND †

January 7, 2009

Abstract. Overlapping Schwarz methods are considered for mixed finite element approximations of linear elasticity, with discontinuous pressure spaces, as well as for compressible elasticity approximated by standard conforming finite elements. The coarse components of the preconditioners are based on spaces, with a number of degrees of freedom per subdomain which is uniformly bounded, and which are similar to those previously developed for scalar elliptic problems and domain decomposition methods of iterative substructuring type, i.e., methods based on non-overlapping decompositions of the domain. The local components of the new preconditioners are based on solvers on a set of overlapping subdomains.

In the current study, the dimension of the coarse spaces is smaller than in recently developed algorithms; in the compressible case all independent face degrees of freedom have been eliminated while in the almost incompressible case five out of six are not needed. In many cases, this will result in a reduction of the dimension of the coarse space by about one half compared to that of the algorithm previously considered. In spite of using overlapping subdomains to define the local components of the preconditioner, only values on the interface between the subdomains need to be retained in the iteration of the new hybrid Schwarz algorithm. The use of discontinuous pressures makes it possible to work exclusively with symmetric, positive definite problems and the standard preconditioned conjugate gradient method.

Bounds are established for the condition number of the preconditioned operators. The bound for the almost incompressible case grows in proportion to the square of the logarithm of the number of degrees of freedom of individual subdomains and the third power of the relative overlap between the overlapping subdomains, and it is independent of the Poisson ratio as well as jumps in the Lamé parameters across the interface between the subdomains. Numerical results illustrate the findings.

Key words. domain decomposition, overlapping Schwarz, preconditioners, iterative methods, almost incompressible elasticity, mixed finite element methods

AMS subject classifications. 65F10, 65N30, 65N55

1. Introduction. We recently considered overlapping Schwarz algorithms for almost incompressible elasticity problems in [10]. Earlier theory for overlapping Schwarz methods for elasticity was restricted to the compressible case in which the Poisson ratio ν is bounded away from its maximum value of $1/2$; see [35, Section 8]. A relatively rich coarse space was used in our recent study, which effectively accommodates all positive values of $\nu < 1/2$. It is an extension of a component of iterative substructuring methods developed about fifteen years ago for scalar elliptic problems; see [12] and also [35, Algorithm 5.16]. Recent applications of such extended coarse spaces to a variety of different problem types appear in [8], and similar algorithms have already been used successfully as part of a production-level iterative solver in the parallel structural dynamics code Salinas [1].

*Sandia National Laboratories, Albuquerque, NM 87185, USA crdohrm@sandia.gov Sandia is a multiprogram laboratory operated by Sandia Corporation, a Lockheed Martin Company, for the United States Department of Energy's National Nuclear Security Administration under contract DE-AC04-94AL85000.

†Courant Institute, 251 Mercer Street, New York NY 10012, USA widlund@cims.nyu.edu, <http://www.cs.nyu.edu/cs/faculty/widlund>. This work was supported in part by the U.S. Department of Energy under contracts DE-FG02-06ER25718 and in part by National Science Foundation Grant DMS-0513251.

In this study, we will only consider problems in three dimensions. In that case, the coarse space of our recent study uses three degrees of freedom for each subdomain vertex, five or six for each subdomain edge and six degrees of freedom for each subdomain face. In this paper, we will show that almost equally strong results can be obtained after switching to a coarse space with only one independent degree of freedom for each subdomain face and that, in fact, all of them can be eliminated in the compressible case. We will also demonstrate that the overlapping subdomains and the Schwarz method that define the local components of the preconditioner can be chosen so that the residuals and iterates need only be retained on the interface of the partitioning of the domain into subdomains. In this respect, our algorithms resemble early work by Barry Smith, see [33, 31] and [35, Algorithm 5.5]. We note that his algorithm uses a conventional finite element space on a coarse triangulation of the domain for the coarse component of the preconditioner.

In the analysis, we focus on our new coarse spaces while the estimates for the local contributions to the preconditioner require essentially no new work; we can borrow what is needed from our recent paper, in particular, from [10, Subsection 5.3]. In this respect, we can benefit from the modular aspects of domain decomposition theory. We also note that, as in our recent work on almost incompressible elasticity, our approach does not require access to individual subdomain matrices, i.e., we can work directly with a globally assembled matrix; this can be an advantage in finite element practice.

An early application of overlapping Schwarz methods to mixed formulations of linear elasticity and incompressible Stokes problems is given in [16]. In that work, the coarse spaces were based on the same mixed finite element methods on coarse meshes and both continuous and discontinuous pressure spaces were considered. An analysis of these methods was not provided, but their performance was shown to be quite competitive with block diagonal and block triangular preconditioners, see [17].

Related iterative substructuring methods as in [35, Chapter 6], for incompressible or almost incompressible problems appear in [7, 13, 21, 22]. For each of these methods, special care is required to ensure that the coarse space is properly constructed. As a result, standard coarse spaces for compressible problems must be modified and enriched to accommodate incompressible or almost incompressible cases.

In this paper, we again restrict our attention to finite elements with discontinuous pressure interpolation. By doing so, it is possible to eliminate the pressure unknowns at the element level. Since the assembled matrix is symmetric and positive definite, an important consequence is that the same solution algorithm, as for compressible elasticity, can be used for the almost incompressible case and that the method of preconditioned conjugate gradients can then be used to accelerate the iteration.

The remainder of this paper is organized as follows. In Section 2, we review the equations of linear elasticity, focusing on the almost incompressible case. We also introduce mixed finite element approximations and then describe the algorithms and formulate the main results in Section 3. These results are proven in Section 4 and results of numerical experiments are given in Section 5.

2. Elasticity and mixed and standard finite elements. Let $\Omega \subset \mathbb{R}^3$ be a domain and let $\partial\Omega_D$ be a nonempty subset of its boundary $\partial\Omega$ and introduce the Sobolev space $\mathbf{V} := \{\mathbf{v} \in \mathbf{H}^1(\Omega) : \mathbf{v}|_{\partial\Omega_D} = 0\}$. Here $\mathbf{H}^1(\Omega) := H^1(\Omega)^3$. The linear elasticity problem consists in finding the displacement $\mathbf{u} \in \mathbf{V}$ of the domain Ω , fixed along $\partial\Omega_D$, and subject to a surface force of density \mathbf{g} , along $\partial\Omega_N = \partial\Omega \setminus \partial\Omega_D$, and

a body force \mathbf{f} :

$$2 \int_{\Omega} \mu \boldsymbol{\epsilon}(\mathbf{u}) : \boldsymbol{\epsilon}(\mathbf{v}) \, dx + \int_{\Omega} \lambda \operatorname{div} \mathbf{u} \operatorname{div} \mathbf{v} \, dx = \langle \mathbf{F}, \mathbf{v} \rangle \quad \forall \mathbf{v} \in \mathbf{V}. \quad (2.1)$$

Here $\lambda(x)$ and $\mu(x)$ are the Lamé parameters, $\epsilon_{ij}(\mathbf{u}) = \frac{1}{2}(\frac{\partial u_i}{\partial x_j} + \frac{\partial u_j}{\partial x_i})$ the linearized strain tensor, and the inner products are defined by

$$\boldsymbol{\epsilon}(\mathbf{u}) : \boldsymbol{\epsilon}(\mathbf{v}) = \sum_{i=1}^3 \sum_{j=1}^3 \epsilon_{ij}(\mathbf{u}) \epsilon_{ij}(\mathbf{v}), \quad \langle \mathbf{F}, \mathbf{v} \rangle = \int_{\Omega} \sum_{i=1}^3 f_i v_i \, dx + \int_{\partial\Omega_N} \sum_{i=1}^3 g_i v_i \, dA.$$

The Lamé parameters can be expressed in terms of the Poisson ratio ν and Young's modulus E :

$$\lambda = \frac{E\nu}{(1+\nu)(1-2\nu)}, \quad \mu = \frac{E}{2(1+\nu)}.$$

The domain Ω is partitioned into non-overlapping subdomains Ω_i . We assume, for simplicity, that the Lamé parameters are constant in each subdomain. Since much of our analysis will be carried out for one subdomain at a time, we can then work with problems with constant coefficients. The bound for the condition number of our algorithm will be independent of the values of all these parameters.

2.1. A saddle point formulation. In the compressible case, we can use standard finite element approximations. However, when the material becomes almost incompressible, the Poisson ratio ν approaches the value $1/2$ and $\lambda/\mu = 2\nu/(1-2\nu)$ approaches infinity. In such cases, finite element discretizations of this pure displacement formulation will increasingly suffer from locking and very slow convergence of the finite element solution.

A well-known remedy is based on introducing the new variable $p = -\lambda \operatorname{div} \mathbf{u} \in U \subset L^2(\Omega)$, that we will call pressure, and replacing the pure displacement problem (2.1) with a mixed formulation: find $(\mathbf{u}, p) \in \mathbf{V} \times U$ such that

$$\left\{ \begin{array}{l} 2 \int_{\Omega} \mu \boldsymbol{\epsilon}(\mathbf{u}) : \boldsymbol{\epsilon}(\mathbf{v}) \, dx - \int_{\Omega} \operatorname{div} \mathbf{v} \, p \, dx = \langle \mathbf{F}, \mathbf{v} \rangle \quad \forall \mathbf{v} \in \mathbf{V} \\ - \int_{\Omega} \operatorname{div} \mathbf{u} \, q \, dx - \int_{\Omega} 1/\lambda \, p q \, dx = 0 \quad \forall q \in U; \end{array} \right. \quad (2.2)$$

see Brezzi and Fortin [4] or Brenner and Scott [3].

In the case of homogeneous Dirichlet boundary conditions for \mathbf{u} on all of $\partial\Omega$, we will choose $U := L_0^2(\Omega) := \{q \in L^2(\Omega) : \int_{\Omega} q \, dx = 0\}$, since it follows from the divergence theorem that the pressure will have a zero mean value. For nonzero Dirichlet boundary data, the same is true if the net flux satisfies $\int_{\partial\Omega} \mathbf{u} \cdot \mathbf{n} \, ds = 0$, where \mathbf{n} is the outward normal. If, on the other hand, the boundary conditions are mixed (part essential and part natural), then there is always a unique solution with a pressure component in $U = L^2(\Omega)$. Rather than discussing two somewhat different cases, we will, from now on, focus on the case with homogeneous Dirichlet boundary conditions on all of $\partial\Omega$.

The net fluxes $\int_{\partial\tilde{\Omega}} \mathbf{u} \cdot \mathbf{n} \, dA$, across the boundary $\partial\tilde{\Omega}$, of subsets $\tilde{\Omega}$ of individual subdomains, will be important in our analysis; see Lemma 4.1. Only if they vanish,

are there divergence-free extensions of the boundary values for which the bilinear form $\int_{\bar{\Omega}} \lambda \operatorname{div} \mathbf{u} \operatorname{div} \mathbf{v} \, dx$ will then vanish.

In our analysis, we will work only with the restrictions of the equations (2.2) to individual subdomains Ω_i , or subsets of such subdomains. In such cases, we can factor out the constants μ_i and $1/\lambda_i$ and we will use the notation $a_i(\mathbf{u}, \mathbf{v})$, $b_i(\mathbf{v}, p)$, and $c_i(p, q)$ for the three resulting bilinear forms associated with the subdomain Ω_i .

In the absence of essential boundary conditions, the elasticity operator has zero energy modes, which are the rigid body modes. There are six of them; they are given in Section 3.

By letting $\lambda_i/\mu_i \rightarrow \infty$, we obtain the limiting problem for incompressible linear elasticity and also a formulation of the Stokes system for incompressible fluids. A penalty term, as in the compressible case, could also originate from stabilization techniques or penalty formulations for Stokes problems.

A Korn inequality for the subspace orthogonal to the rigid body modes establishes an equivalence between the square of the semi-norm in $\mathbf{H}^1(\Omega_i)$ and the bilinear form $a_i(\cdot, \cdot)$; see further Lemma 4.1. This will make it possible to use many tools and results developed in studies of scalar elliptic problems.

2.2. Mixed finite element methods with discontinuous pressures. We assume that the domain Ω is decomposed into N non-overlapping subdomains Ω_i of diameter H_i . The interface of this decomposition is given by

$$\Gamma = \left(\bigcup_{i=1}^N \partial\Omega_i \right) \setminus \partial\Omega.$$

To simplify the discussion, we will assume, as in [35, Assumption 4.3], that each subdomain is the union of shape-regular tetrahedral elements of a global conforming coarse mesh and that the number of such tetrahedra forming any individual subdomain is uniformly bounded. We note that this assumption makes the subdomains shape regular, i.e., they have bounded aspect ratios. This assumption makes it possible to use all the technical tools developed in [35, Section 4.6] in the analysis. Each subdomain is further partitioned into many shape-regular elements. We assume that the nodes match across the interface between the subdomains and we denote the set of elements by \mathcal{T}_h . We note that recent advances in the analysis of domain decomposition methods defined on quite irregular subdomains would allow us to extend all our results, in the case of two dimensions, to very irregular subdomains that are only *John domains*; see [10, Section 6] and [9, 19].

In our experimental work, we have chosen to work primarily with the $Q_2(h) - P_1(h)$ finite elements: the displacement space is $\mathbf{V}^h := (Q_2(h))^3$, while the pressure space consists of discontinuous, piecewise linear functions:

$$U^h := \{q \in U : q|_T \in P_1(T) \quad \forall T \in \mathcal{T}_h\}.$$

The two spaces are defined on the same hexahedral mesh. This mixed finite element method satisfies a uniform inf-sup condition:

$$\sup_{\mathbf{v} \in \mathbf{V}^h} \frac{b_i(\mathbf{v}, q)}{a_i(\mathbf{v}, \mathbf{v})^{1/2}} \geq \beta c_i(q, q)^{1/2} \quad \forall q \in U_i^h \cap L_0^2(\Omega_i), \quad \beta > 0. \quad (2.3)$$

The parameter β depends on the domain and, in particular, it varies inversely with the aspect ratio of the domain; these matters are discussed at length in [10, Subsections

5.2 and 5.3]. This is the origin of two factors, $(1 + (H/\delta))^2$, in our condition number bound in the almost incompressible case. There are optimal $O(h^2)$ error estimates for both displacements and pressures for this mixed finite element method; see Brezzi and Fortin [4, chap. VI, p. 216].

We note that while finite element methods based on hexahedra and quadrilaterals enjoy popularity, our theory applies equally well to any stable mixed method, e.g., one based on tetrahedral elements as long as the pressure space is discontinuous. We could also consider more general saddle point problems with penalty terms.

In matrix form, the mixed finite element approximation for subdomain Ω_i will contribute the stiffness matrix

$$\begin{bmatrix} \mu_i A^{(i)} & B^{(i)T} \\ B^{(i)} & (-1/\lambda_i) C^{(i)} \end{bmatrix}. \quad (2.4)$$

At the expense of solving a small linear system of equations for each individual element, we can define a reduced, positive definite, symmetric system matrix

$$\tilde{A}^{(i)} = \mu_i A^{(i)} + \lambda_i B^{(i)T} C^{(i)-1} B^{(i)}. \quad (2.5)$$

Just as in the compressible case, these submatrices can be assembled into \tilde{A} , which represents the energy of the entire system. The corresponding bilinear forms are denoted by $\tilde{a}_i(\cdot, \cdot)$ and $\tilde{a}(\cdot, \cdot)$.

3. The algorithm and the main results. We will describe and analyze our algorithm as a two-level Schwarz method, as in [35, Chapters 2, 3, and 5], defined in terms of a set of subspaces. We focus on the more complicated almost incompressible case; the compressible case needs only to be discussed briefly. In the almost incompressible case, we will work with the displacement variables only and the positive definite formulation (2.5) obtained after all pressure degrees of freedom are eliminated.

3.1. The subspaces of the Schwarz algorithm. We will use a smaller coarse space \mathbf{V}_0 than in our recent study [10], and a pair of local spaces \mathbf{V}_i and $\mathbf{V}_{i\delta}$ associated with each subdomain Ω_i . This choice and the selection of special hybrid Schwarz algorithms will make it possible to retain only the interface values of the residuals and conjugate gradient iterates.

As the subdomains, which define the local components of the overlapping Schwarz preconditioner, we will use the nonoverlapping subdomains Ω_i into which the given domain Ω has been subdivided. We note that the resulting Dirichlet solvers on these subdomains are also used to compute the coarse basis functions of our algorithm from their boundary values. Additionally, we will also use *necklace* subdomains $\Omega_{i\delta}$ constructed from an integer number of layers of elements around the local interface $\Gamma_i := \partial\Omega_i \cap \Gamma$; see Fig. 5.1, right, for a three-dimensional picture. Each of these subdomains is characterized by a parameter δ_i , which is the distance from Γ_i to $\partial\Omega_{i\delta} \setminus \partial\Omega$. We note that for small overlap, the factorization of the stiffness matrices for the $\Omega_{i\delta}$ can be considerably less expensive than that for the subdomain Ω_i . We note that domain decomposition preconditioners of *interface-strip* type have been considered in [28, 29]. The global components of these preconditioners are obtained from solvers of problems defined on the union of all the $\Omega_{i\delta}$ and they therefore differ from ours.

We build the local components of our Schwarz preconditioner by restricting the original problem to the subdomains Ω_i and $\Omega_{i\delta}$, in the customary way, and by solving Dirichlet problems with zero boundary data to obtain related local corrections.

All elements of the coarse space are discrete saddle-point harmonic functions in the sense that they are minimal energy extensions of values given on the interface; in the almost incompressible case they are computed by solving a Dirichlet problem for each Ω_i using matrices obtained from $\tilde{A}^{(i)}$.

DEFINITION 3.1. *The discrete saddle-point harmonic function for boundary data w_Γ has the vector representation*

$$w_{sh} = \begin{bmatrix} w_I \\ w_\Gamma \end{bmatrix},$$

where w_I is given by the solution of

$$\begin{bmatrix} \mu_i A_{II}^{(i)} & B_I^{(i)T} \\ B_I^{(i)} & (-1/\lambda_i)C^{(i)} \end{bmatrix} \begin{bmatrix} w_I \\ q \end{bmatrix} = \begin{bmatrix} -\mu_i A_{I\Gamma}^{(i)} w_\Gamma \\ -B_\Gamma^{(i)} w_\Gamma \end{bmatrix}. \quad (3.1)$$

Here, $A_{II}^{(i)}$ is a leading principal minor of $A^{(i)}$, if the interior variables are all ordered ahead of those of the interface, $A_{I\Gamma}^{(i)}$ represents the coupling between the interface and the interior, etc.

To introduce the coarse space \mathbf{V}_0 , we first decompose the local interfaces Γ_i into faces \mathcal{F}^{ij} , edges \mathcal{E}^{ik} , and vertices $\mathcal{V}^{i\ell}$. A face is an open subset of Γ_i and an edge is an open subset of the boundaries of several faces. A node on \mathcal{F}^{ij} is common to two subdomains Ω_i and Ω_j while those on an edge typically are common to more than two. The vertices are endpoints of the edges. For an additional discussion of how to define these sets, even for very irregular subdomains, see [6, 18, 20].

The smaller coarse component space is similar to that of the algorithm studied in [10]. In turn, it was adapted from older iterative substructuring algorithms described in [35, Section 5.4] and first developed for scalar elliptic problems in [12]. Because of the larger null space of the elasticity operator, the coarse space must be enriched to make it work for elasticity; see [35, Sections 8.3 and 8.4]. This is related to the well-known null space property, which is necessary to obtain scalability, i.e., a bound on the convergence, which does not depend on the number of subdomains; see the discussion in [23] or [34].

The rigid body modes are three translations

$$\mathbf{r}_1 := \begin{bmatrix} 1 \\ 0 \\ 0 \end{bmatrix}, \mathbf{r}_2 := \begin{bmatrix} 0 \\ 1 \\ 0 \end{bmatrix}, \mathbf{r}_3 := \begin{bmatrix} 0 \\ 0 \\ 1 \end{bmatrix}, \quad (3.2)$$

and three rotations

$$\mathbf{r}_4 := \frac{1}{H_i} \begin{bmatrix} 0 \\ -x_3 + \hat{x}_3 \\ x_2 - \hat{x}_2 \end{bmatrix}, \mathbf{r}_5 := \frac{1}{H_i} \begin{bmatrix} x_3 - \hat{x}_3 \\ 0 \\ -x_1 + \hat{x}_1 \end{bmatrix}, \mathbf{r}_6 := \frac{1}{H_i} \begin{bmatrix} -x_2 + \hat{x}_2 \\ x_1 - \hat{x}_1 \\ 0 \end{bmatrix}, \quad (3.3)$$

where $\hat{x} \in \Omega_i$ can be chosen as a midpoint of an edge or face. The shift of the origin makes this basis for the space of rigid body modes well conditioned, and the scaling and shift make these six functions scale in the same way with H_i . This ensures that the norms of the six functions are comparable.

The coarse basis functions for the algorithm in [10] can be defined by using cutoff functions $\theta_{\mathcal{F}^{ij}}$, $\theta_{\mathcal{E}^{ik}}$ and $\theta_{\mathcal{V}^{i\ell}}$. The face function $\theta_{\mathcal{F}^{ij}}$ equals 1 at all the nodes of the face and vanishes at all other nodes on the interface. The edge functions $\theta_{\mathcal{E}^{ik}}$ and vertex functions $\theta_{\mathcal{V}^{i\ell}}$ are defined similarly.

For each face, we can use the finite element interpolant of the product of this face cutoff function and the rigid body modes to obtain six linearly independent functions $I^h(\theta_{\mathcal{F}^{ij}}\mathbf{r}_k)$; we extend the resulting boundary values into the interior of the subdomains as discrete saddle-point harmonic functions. Here, I^h is the interpolation operator, which maps onto the finite element space \mathbf{V}^h . The boundary values for these functions, which are all used as coarse basis functions in [10], can also be obtained by restricting the rigid body modes to the nodes of \mathcal{F}^{ij} and setting the values at all other interface nodes to zero.

Similarly, for a straight edge, we obtain five linearly independent rigid body modes since, as is easy to see, a rigid body mode representing a rotation, with the edge as its axis, is invisible on the edge; for a detailed discussion of the case of curved edges, for which we use six degrees of freedom, see [18]. In [10], we thus use coarse basis functions associated with the edge which are given as $I^h(\theta_{\mathcal{E}^{ik}}\mathbf{r})$ where $\mathbf{r} \in \mathcal{RB}$.

For each vertex, finally, we have three degrees of freedom representing the displacement at that point.

We will now modify this coarse space and eliminate most of the independent face coarse degrees of freedom. The construction is inspired by earlier work on wire basket based methods and in particular by [27] which in turn builds on [32, 2]; see also [35, pp. 222-223].

We consider one face \mathcal{F}^{ij} at a time and one rigid body mode \mathbf{r}_m , which defines one of the edge coarse basis functions given above. We will obtain the corresponding modified edge coarse basis function by extending its values to the faces which have this edge in common. The same kind of extension will be used for each subdomain vertex.

The face contributions to these modified edge and vertex functions are of the form

$$\sum_{\ell=1}^6 \alpha_{\ell m} I^h(\theta_{\mathcal{F}^{ij}}\mathbf{r}_\ell).$$

To determine the coefficients $\alpha_{\ell m}$, for a modified edge basis function, we solve a least squares problem:

$$\min_{\alpha_{\ell m}} \|I^h(\theta_{\mathcal{E}^{ik}}\mathbf{r}_m) - \sum_{\ell=1}^6 \alpha_{\ell m} \mathbf{r}_\ell\|_{\mathbf{L}^2(\partial\mathcal{F}^{ij})}^2.$$

Here, $\mathbf{L}^2(\partial\mathcal{F}^{ij}) = L^2(\partial\mathcal{F}^{ij})^3$. We define the values of the modified vertex basis functions in the same way.

It is elementary to show that $\mathbf{L}^2(\partial\mathcal{F}^{ij})$ -norm of $\sum_1^6 \alpha_{\ell m} \mathbf{r}_\ell$ will be less than or equal to that of $I^h(\theta_{\mathcal{E}^{ik}}\mathbf{r}_m)$.

Since the rigid body modes are linearly independent, it is easy to prove the following lemma:

LEMMA 3.2. *The coefficients $\alpha_{\ell m}$ of any of the modified coarse edge basis function are all $O(1)$ and those for the coarse vertex basis functions are all $O(h_i/H_i)$.*

By using this lemma, [35, Lemma 4.25], and an elementary estimate of the energy of $I^h(\theta_{\mathcal{F}^{ij}}\mathbf{r}_\ell)$, we find that

LEMMA 3.3. *The square of the \mathbf{H}^1 -norm of the modified coarse edge basis functions are bounded by $C(1 + \log(H_i/h_i))H_i$. Similarly, the square of the norm of any modified coarse vertex basis function can be bounded by $C(1 + \log(H_i/h_i))h_i$.*

We note that the energy of these modified basis functions exceed those of the original edge functions by a factor $(1 + \log(H/h))$. It is clear from our construction

that, when restricted to an interior subdomain, this coarse space will contain all the rigid body modes. As previously noted, this is a requirement for obtaining a scalable algorithm; see, e.g., [35, Section 8.2].

We note that in practice, we can find good weights $\alpha_{\ell m}$, to define the extension of the edge and vertex coarse basis functions to the interior nodes of the face, by replacing the \mathbf{L}^2 -norm over the boundary of the face by an ℓ^2 -norm over the values at the nodes of the same set. Lemmas 3.2 and 3.3 are still valid.

We have now constructed a complete coarse space for the compressible case. For the almost incompressible case, we will add one independent coarse basis function for each face. For a flat face, we choose a *face bubble function* $\theta_{\mathcal{F}^{ij}} \mathbf{n}_{\mathcal{F}^{ij}}$ where $\mathbf{n}_{\mathcal{F}^{ij}}$ is a unit normal to the face. We note that this function is linearly independent of the edge and vertex basis functions since it vanishes on the boundary of the face while the modified edge and vertex functions do not.

We can also define a suitable average normal direction for a curved face by first constructing a matrix with three columns and where each row contains the three coordinates of a node on \mathcal{F}^{ij} . We then shift the origin of the coordinate system so that the average of the elements of each of the columns vanishes. By computing the singular value decomposition $U\Sigma V^T$ of this matrix, we will, in particular, find the orthogonal matrix V of order 3. Its third column, the right singular vector associated with the smallest singular value, will be our choice. It is the normal to the plane through the origin, after the shift, for which the sum of the squares of the distance of the nodes on the curved face to the plane is minimized.

3.2. A hybrid Schwarz algorithm. We need to specify the Schwarz method used. We recall the definition of the projections from which the Schwarz method is built; for simplicity, we will assume that exact solvers are used for the local problems defined on the overlapping subdomains as well as for the global, coarse problem. We also recall that $\tilde{a}(\cdot, \cdot)$ is the displacement-only bilinear form for the entire domain Ω and that $\tilde{a}_i(\cdot, \cdot)$ is that for subdomain Ω_i . For any $i \geq 1$, we use an extension operator $R_i^T : \mathbf{V}_i \rightarrow \mathbf{V}^h$; this is a simple extension by zero to the nodes not in Ω_i . Extension operators $R_{i\delta}^T$ are defined similarly and R_0^T imbeds \mathbf{V}_0 into \mathbf{V}^h .

Associated with the coarse space is a projection $P_0 : \mathbf{V}^h \rightarrow \mathbf{V}_0$; it is orthogonal with respect to the $\tilde{a}(\cdot, \cdot)$ -inner product. For the local spaces \mathbf{V}_i and $\mathbf{V}_{i\delta}$, there are projections $P_i : \mathbf{V}^h \rightarrow R_i^T \mathbf{V}_i$ and $P_{i\delta} : \mathbf{V}^h \rightarrow R_{i\delta}^T \mathbf{V}_{i\delta}$ defined by

$$P_i = R_i^T \tilde{P}_i \quad \text{with } \tilde{P}_i \text{ defined by } \tilde{a}_i(\tilde{P}_i \mathbf{u}, \mathbf{v}) = \tilde{a}(\mathbf{u}, R_i^T \mathbf{v}) \quad \forall \mathbf{v} \in \mathbf{V}_i,$$

and

$$P_{i\delta} = R_{i\delta}^T \tilde{P}_{i\delta} \quad \text{with } \tilde{P}_{i\delta} \text{ defined by } \tilde{a}_{i\delta}(\tilde{P}_{i\delta} \mathbf{u}, \mathbf{v}) = \tilde{a}(\mathbf{u}, R_{i\delta}^T \mathbf{v}) \quad \forall \mathbf{v} \in \mathbf{V}_{i\delta}.$$

Recall that $\tilde{a}_i(\cdot, \cdot)$ has already been defined; we can define $\tilde{a}_{i\delta}(\cdot, \cdot)$ similarly.

In this study, we use a Schwarz method of hybrid type; cf. [35, Subsection 2.5.2]; we note that [35, Chapter 2] provides an introduction to the abstract theory of Schwarz methods. An early example of such a hybrid Schwarz method is the Neumann–Neumann algorithm as described in [25] and [35, Section 6.2]. In that algorithm, a coarse space correction is computed in the first and third of three fractional steps, while the rest of the corrections are handled as in an additive Schwarz method. Here we will instead consider the Schwarz method based on the polynomial

$$P_{hyb} := \left(I - \sum_{i=1}^N P_i \right) \left(P_0 + \sum_{i=1}^N P_{i\delta} \right) \left(I - \sum_{i=1}^N P_i \right). \quad (3.4)$$

Just as in the case discussed in [35, Subsection 2.5.2], the first factor is a projection; this follows from the observation that the P_i are projections and that $P_i P_j = 0, i \neq j$.

The application of the third (and first) factor of (3.4) eliminates all residuals interior to the subdomains Ω_i resulting in piecewise discrete saddle-point harmonic functions and thus defined fully in terms of their values on the interface Γ . By eliminating all residuals in the interior of the subdomains initially, all the residuals of the conjugate gradient iteration will be discrete saddle-point harmonic. We also note that from the second iteration on, we only need to apply the operator $(I - \sum_{i=1}^N P_i)$ once in each step of the iteration.

We find that we essentially only have to estimate the parameter C_0^2 of the standard Schwarz theory, as developed in [35, Section 2.3],

$$\tilde{a}(\mathbf{u}_0, \mathbf{u}_0) + \sum_{i=1}^N \tilde{a}_i(\mathbf{u}_i, \mathbf{u}_i) + \sum_{i=1}^N \tilde{a}_{i\delta}(\mathbf{u}_{i\delta}, \mathbf{u}_{i\delta}) \leq C_0^2 \tilde{a}(\mathbf{u}, \mathbf{u}) \quad \forall \mathbf{u} \in \mathbf{V}^h, \quad (3.5)$$

for some choice of $\{\mathbf{u}_i\}_0^N, \mathbf{u}_i \in \mathbf{V}_i$ and $\{\mathbf{u}_{i\delta}\}_1^N, \mathbf{u}_{i\delta} \in \mathbf{V}_{i\delta}$, such that

$$\mathbf{u} = \sum_{i=0}^N R_i^T \mathbf{u}_i + \sum_{i=1}^N R_{i\delta}^T \mathbf{u}_{i\delta}. \quad (3.6)$$

A lower bound on C_0^{-2} provides, as always, a lower bound for the additive Schwarz method, based on these subspaces. It is also known that the lower bound of P_{hyb} is at least as good as that of the additive method; see [24] or [35, Lemma 2.15].

An upper bound of the norm of $P_0 + \sum_1^N P_{i\delta}$ is obtained by a standard coloring argument as in [35, Subsection 2.5.1]. Since the first and third factors of P_{hyb} are projections, they do not contribute to the bound of the norm of our hybrid Schwarz operator. Thus, we obtain a constant upper bound for P_{hyb} .

Our main result, obtained by estimating C_0^2 , is:

THEOREM 3.4 (Almost incompressible elasticity). *The condition number of our domain decomposition method, which uses one independent face coarse degree of freedom for each face of Γ , satisfies*

$$\kappa(P_{hyb}) \leq C(1 + (H/\delta))^3(1 + \log(H/h))^2.$$

Here C is a constant which is independent of the number of subdomains and their diameters, the mesh size, and the values of the Lamé parameters. It depends only on the shape regularity of the elements and the subdomains.

As in many domain decomposition results, H/h is shorthand for $\max_i(H_i/h_i)$, where h_i is the smallest diameter of the elements of Ω_i . Similarly, H/δ is the largest ratio of H_i and δ_i .

We also have a result for the compressible case:

THEOREM 3.5 (Compressible elasticity). *The condition number of our domain decomposition method, without any independent coarse face degrees of freedom, satisfies*

$$\kappa(P_{hyb}) \leq C(1 + (H/\delta))(1 + \log(H/h))^2.$$

Here C is a constant, independent of the number of subdomains and their diameters and the mesh size. It depends only on the shape regularity of the elements and the subdomains.

4. Proofs of the main results. We first note that for the case of the richer coarse space considered in [10], there is essentially nothing new to prove in case we use the subdomains $\Omega_{i\delta}$ and the original subdomains Ω_i to define the local components of the preconditioner; see further Subsection 4.2. We will therefore focus on the effects of the smaller coarse space and derive an interpolation formula onto that space based on the discussion and results of Subsection 3.1.

As in the theory for iterative substructuring algorithms, see [35, Chapters 4, 5, and 6], the analysis can be carried out for one subdomain Ω_i at a time and variations in the values of the Lamé parameters between subdomains will therefore not enter our bounds.

We recall that the coarse space, restricted to an individual subdomain that does not touch $\partial\Omega$, will contain all rigid body modes and that we have constructed a basis for the coarse space in terms of these modes and cutoff functions associated with the faces, edges, and vertices of the subdomain Ω_i . When constructing the coarse space component \mathbf{u}_0 , by a specific interpolation procedure, we will make sure that all rigid body modes are reproduced and also that the remainder, $\mathbf{w} = \mathbf{u} - \mathbf{u}_0$, will have a zero net flux across all the faces of the interface. Our construction and estimates can be used both for interior subdomains and for those with a boundary that intersects $\partial\Omega$; our interpolation procedure will reproduce the zero Dirichlet boundary condition on $\partial\Omega_i \cap \partial\Omega$.

To assure that the zero net flux condition holds, in the almost incompressible case, we will, in a final step, introduce and estimate face corrections using the remaining, independent coarse face basis functions. The correction is of the form

$$\mathbf{u}_0^f = \sum_{ij} \beta_{ij} \theta_{\mathcal{F}^{ij}} \mathbf{n}_{\mathcal{F}^{ij}},$$

where the β_{ij} are chosen so that

$$\beta_{ij} \int_{\mathcal{F}^{ij}} \theta_{\mathcal{F}^{ij}} dA = \int_{\mathcal{F}^{ij}} (\mathbf{u} - \mathbf{u}_0^v - \mathbf{u}_0^e) \cdot \mathbf{n}_{\mathcal{F}^{ij}} dA. \quad (4.1)$$

Here \mathbf{u}_0^v and \mathbf{u}_0^e are the sum of the vertex and edge components of \mathbf{u}_0 . We obtain \mathbf{u}_0 as the sum of the three terms.

The coarse interpolant \mathbf{u}_0 is chosen so that we can estimate $\tilde{a}_i(\mathbf{u} - \mathbf{u}_0, \mathbf{u} - \mathbf{u}_0)$ in terms of $a_i(\mathbf{u} - \mathbf{u}_0, \mathbf{u} - \mathbf{u}_0)$, by using the following lemma, which has a constant which is uniformly bounded for all values of the potentially large parameter λ_i .

LEMMA 4.1. *Let \mathbf{u}_{sh} denote the discrete saddle-point harmonic function with the same boundary data as \mathbf{u} on $\partial\Omega_i$ and which satisfies the zero net flux condition*

$$\int_{\partial\Omega_i} \mathbf{u} \cdot \mathbf{n} ds = 0.$$

Then,

$$\tilde{a}_i(\mathbf{u}_{sh}, \mathbf{u}_{sh}) \leq 4 \left(1 + \frac{n/2}{\mu_i/\lambda_i + \beta^2} \right) a_i(\mathbf{u}, \mathbf{u}) \quad \forall \mathbf{u} \in \mathbf{V}^h. \quad (4.2)$$

For a proof of a closely related result, see [10, Lemma 3.3].

By using this estimate, we can rely on standard technical tools collected in [35, Section 4.6] and [20, Section 7]; they were developed for scalar elliptic problems and compressible elasticity, respectively.

4.1. The coarse component of the decomposition. The construction of \mathbf{u}_0 begins by setting $\mathbf{u}_0(\mathcal{V}^{i\ell}) = \mathbf{u}(\mathcal{V}^{i\ell})$ at all vertices of the subdomain. While $\mathbf{u} - \mathbf{u}_0$ will vanish at all subdomain vertices, we have to estimate the contributions from the vertex coarse basis functions, which differ from zero on the faces next to a vertex. We use an inverse inequality given in [35, Formula (4.16)]:

$$\|u_h\|_{L^\infty(\Omega_i)}^2 \leq (C/h_i) \|u_h\|_{H^1(\Omega_i)}^2$$

to estimate $\mathbf{u}_0(\mathcal{V}^{i\ell})$. Combining this estimate with Lemma 3.3, find that

$$|\mathbf{u}_0^v|_{\mathbf{H}^1(\Omega_i)} \leq C(1 + \log(H_i/h_i)) \|\mathbf{u}_h\|_{\mathbf{H}^1(\Omega_i)}^2.$$

Next, for each edge \mathcal{E}^{ik} of Ω_i , we select the coefficients for the modified edge basis elements such that

$$(\mathbf{u} - \mathbf{u}_0, \mathbf{r})_{\mathbf{L}^2(\mathcal{E}^{ik})} = 0 \quad \forall \mathbf{r} \in \mathcal{RB}.$$

We note that, since an edge component is obtained by restricting rigid body modes to the nodes of the edge and $\mathbf{u} - \mathbf{u}_0$ vanishes at the subdomain vertices, we can also find that component by solving

$$\inf_{\mathbf{r} \in \mathcal{RB}} \|I^h(\theta_{\mathcal{E}^{ik}}(\mathbf{u} - \mathbf{r}))\|_{\mathbf{L}^2(\mathcal{E}^{ik})}^2. \quad (4.3)$$

A bound on the square of the ℓ^2 -norm of the vector of coefficients of the coarse edge basis functions of \mathbf{u}_0^e can then be given by $(C/H_i) \|\mathbf{u}\|_{\mathbf{L}^2(\mathcal{E}^{ik})}^2$. By using Lemma 3.3, we find that

$$|\mathbf{u}_0^e|_{\mathbf{H}^1(\Omega_i)}^2 \leq C(1 + \log(H_i/h_i)) \|\mathbf{u}\|_{\mathbf{L}^2(\mathcal{E}^{ik})}^2.$$

We can estimate the right hand side of this inequality by using [35, Lemma 4.16] and obtain

$$|\mathbf{u} - \mathbf{u}_0^v - \mathbf{u}_0^e|_{\mathbf{H}^1(\Omega_i)}^2 \leq C(1 + \log(H_i/h_i))^2 \|\mathbf{u}\|_{\mathbf{H}^1(\Omega_i)}^2.$$

We also have to estimate for \mathbf{u}_0^f , the correction term given in terms of the remaining independent face coarse degrees of freedom. Turning to formula (4.1), we find, by using the Cauchy-Schwarz inequality, that

$$|\beta_{ij}|^2 \leq C/H_i^2 \|\mathbf{u} - \mathbf{u}_0^v - \mathbf{u}_0^e\|_{\mathbf{L}^2(\mathcal{F}^{ij})}^2.$$

We now use an elementary trace theorem, see [26, Theorem 1.2], and a scaling argument to show that

$$C/H_i^2 \|\mathbf{u}\|_{\mathbf{L}^2(\mathcal{F}^{ij})}^2 \leq C/H_i \|\mathbf{u}\|_{\mathbf{H}^1(\Omega_i)}^2.$$

We also note that

$$C/H_i^2 \|\mathbf{u}_0^v + \mathbf{u}_0^e\|_{\mathbf{L}^2(\mathcal{F}^{ij})}^2$$

can be bounded by Ch_i^2 times the square of the ℓ^2 -norm of the coefficients of the modified vertex coarse basis functions plus C times the square of the ℓ^2 -norm of the coefficients of the modified edge coarse basis functions. By using the same arguments

as before, we obtain bounds for these coefficients in terms of the $\mathbf{H}^1(\Omega_i)$ -norm of \mathbf{u} and finally a bound for $|\mathbf{u}_0^f|_{\mathbf{H}^1(\Omega_i)}^2$. We can conclude that

$$|\mathbf{u} - \mathbf{u}_0|_{\mathbf{H}^1(\Omega_i)}^2 \leq C(1 + \log(H_i/h_i))^2 \|\mathbf{u}\|_{\mathbf{H}^1(\Omega_i)}^2. \quad (4.4)$$

We note that one of the logarithmic factors reflects the bound of the energy of the modified coarse vertex and edge basis functions; cf. Lemma 3.3.

We will now use the following lemma

LEMMA 4.2. *Let Ω_i be a Lipschitz domain of diameter H_i . Then, there exists a constant $C = C(\Omega_i)$ such that*

$$\inf_{\mathbf{r} \in \mathcal{RB}} \|\mathbf{v} - \mathbf{r}\|_{\mathbf{H}^1(\Omega_i)}^2 \leq C a_i(\mathbf{v}, \mathbf{v}).$$

This is [10, Lemma 5.2]; it is obtained by using Korn's second inequality and a Poincaré inequality.

Our recipe for \mathbf{u}_0 will clearly reproduce any rigid body mode. We can therefore replace the square of the norm on the right hand side of (4.4) by $\inf_{\mathbf{r} \in \mathcal{RB}} \|\mathbf{u} - \mathbf{r}\|_{\mathbf{H}^1(\Omega_i)}^2$ and then, by using Lemma 4.2, by $a_i(\mathbf{u}, \mathbf{u})$.

We now consider $\tilde{a}_i(\mathbf{u} - \mathbf{u}_0, \mathbf{u} - \mathbf{u}_0)$. Since the net flux across $\partial\Omega_i$ of $\mathbf{u} - \mathbf{u}_0$ vanishes, we can use Lemma 4.1 and estimate this expression by

$$4 \left(1 + \frac{n/2}{\mu_i/\lambda_i + \beta^2} \right) \mu_i a_i(\mathbf{u} - \mathbf{u}_0, \mathbf{u} - \mathbf{u}_0).$$

By using the elementary estimate

$$a_i(\mathbf{v}, \mathbf{v}) = 2 \int_{\Omega_i} \varepsilon(\mathbf{v}) : \varepsilon(\mathbf{v}) dx \leq 2 |\mathbf{v}|_{\mathbf{H}^1(\Omega_i)}^2,$$

this expression, in turn, can be estimated by

$$8 \left(1 + \frac{n/2}{\mu_i/\lambda_i + \beta^2} \right) \mu_i |\mathbf{u} - \mathbf{u}_0|_{\mathbf{H}^1(\Omega_i)}^2$$

and therefore, by using (4.4) and Lemma 4.2, also by $C(1 + \log(H_i/h_i))^2 \mu_i a_i(\mathbf{u}, \mathbf{u})$. We can then return to the \tilde{a}_i -norm by using the elementary inequality

$$\mu_i a_i(\mathbf{u}, \mathbf{u}) \leq \tilde{a}_i(\mathbf{u}, \mathbf{u}).$$

A bound for $\tilde{a}_i(\mathbf{u}_0, \mathbf{u}_0)$ follows from

$$\tilde{a}_i(\mathbf{u}_0, \mathbf{u}_0) \leq 2\tilde{a}_i(\mathbf{u} - \mathbf{u}_0, \mathbf{u} - \mathbf{u}_0) + 2\tilde{a}_i(\mathbf{u}, \mathbf{u})$$

and a bound,

$$\tilde{a}_i(\mathbf{u}_0, \mathbf{u}_0) \leq C(1 + \log(H/h))^2 \tilde{a}_i(\mathbf{u}, \mathbf{u}), \quad (4.5)$$

then results by adding the contributions from all the substructures and using the bound for the contributions from the substructures.

4.2. The local components of the decomposition. We will now show how certain constructions and estimates provided in [10, Subsection 5.3] can be used to find the local components $\mathbf{u}_i \in \mathbf{V}_i, i \geq 1$ and $\mathbf{u}_{i\delta} \in \mathbf{V}_{i\delta}$ in the decomposition of $\mathbf{w} = \mathbf{u} - \mathbf{u}_0$ and to find an estimate of the parameter C_0^2 in (3.5). As in our previous paper, [10], we can focus on the contributions of one subdomain Ω_i and show how to partition \mathbf{w} in Ω_i . We note that \mathbf{w} , by construction, vanishes at all vertices of the subdomains. We also note that while we use a different formula for \mathbf{u}_0 than in [10], there are no new difficulties in the analysis.

For each face \mathcal{F}^{ij} of Ω_i , we consider the intersection of $\Omega_{i\delta}$ and $\Omega_{j\delta}$. In [10] a function $\mathbf{w}_{\mathcal{F}^{ij}}$ is constructed, which satisfies the no net flux condition across the face, vanishes on the rest of the interface Γ , and is supported in the closure of this intersection. We allocate $(1/2)\mathbf{w}_{\mathcal{F}^{ij}}$ to each of $\mathbf{u}_i \in \mathbf{V}_{i\delta}$ and $\mathbf{u}_j \in \mathbf{V}_{j\delta}$ and we can then use a bound established in [10]:

$$\tilde{a}_i(\mathbf{w}_{\mathcal{F}^{ij}}, \mathbf{w}_{\mathcal{F}^{ij}}) \leq C(1 + (H_i/\delta_i))^3(1 + \log(H_i/h_i))^2 \tilde{a}_i(\mathbf{u}, \mathbf{u}). \quad (4.6)$$

Similarly, for each edge \mathcal{E}^{ik} of Ω_i , we consider the intersection Ψ_{ik} of all $\Omega_{k\delta}$ for which \mathcal{E}^{ik} is an edge of Ω_k . In [10], we have constructed a function $\mathbf{w}_{\mathcal{E}^{ik}}$, which satisfies the no net flux condition across the two faces of Ω_i which share the edge, and which is supported in the closure of Ψ_{ik} . The following estimate is also established in [10]:

$$\tilde{a}_i(\mathbf{w}_{\mathcal{E}^{ik}}, \mathbf{w}_{\mathcal{E}^{ik}}) \leq C(1 + (H_i/\delta_i))^2(1 + \log(H_i/h_i)) \tilde{a}_i(\mathbf{u}, \mathbf{u}). \quad (4.7)$$

If p subdomains Ω_k have that edge in common, we allocate $(1/p)\mathbf{w}_{\mathcal{E}^{ik}}$ to each of the relevant $\mathbf{V}_{k\delta}$.

We note that all these functions, $\mathbf{w}_{\mathcal{F}^{ij}}$ and $\mathbf{w}_{\mathcal{E}^{ik}}$, are extended as continuous functions across $\partial\Omega_i$ if the same construction is used for the other subdomains; see [10, Subsection 5.3]. The sum of these face and edge functions for the subdomain Ω_i equals \mathbf{w} on $\partial\Omega_i$. We can therefore choose $\mathbf{u}_i \in \mathbf{V}_i$, in the decomposition of \mathbf{w} , as what remains of \mathbf{w} after that all these face and edge functions have been subtracted from it. By using (4.6) and (4.7), we can find a bound of the same quality for $\tilde{a}_i(\mathbf{u}_i, \mathbf{u}_i)$.

Combining the resulting estimates with the estimate of $\tilde{a}(\mathbf{u}_0, \mathbf{u}_0)$ given in (4.5), we have a bound for C_0^2 , and have thus completed the proof of the lower bound for the Schwarz operator P_{hyb} , and the proof of Theorem 3.4.

4.3. The compressible elasticity case. The proof of Theorem 3.5 essentially only requires arguments that have been used previously to analyze Schwarz methods based on overlapping subdomains; see, e.g., [35, Chapter 3]. A variant of these arguments are used in [9] in which the older theory is extended to the case with large variations of the coefficients across the interface. We note that the logarithmic factors in Theorem 3.5 originate from the bound of \mathbf{u}_0 .

We also note that we can establish the same result as in Theorem 3.4 in case we approximate some subdomains, where the material is compressible, with a standard finite element method and others with a mixed finite element method as in this paper. All that is required is that the finite element meshes and degrees of freedom match across the interface and that we have that extra independent coarse face degree of freedom for all faces of the subdomains which are almost incompressible.

5. Numerical Results. Results are presented in this section to confirm the theory and to demonstrate the usefulness of our algorithm. Attention is restricted primarily to meshes of inf-sup stable $Q_2 - P_1$ hexahedral elements, but we also consider

lower-order $Q_1 - P_0$ elements in some cases. The $Q_1 - P_0$ element is not inf-sup stable and could have convergence issues for Poisson ratios close to $1/2$, but it is often used in practice for reasons of convenience. We note that it is equivalent to a standard displacement-based Q_1 elasticity element with selective reduced integration of bulk strain energy; see, e.g., [15, Section 4.4]. Pressure unknowns can be eliminated at the element level for both $Q_2 - P_1$ and $Q_1 - P_0$ if the Poisson ratio is less than $1/2$.

Unless specified otherwise, the results presented are for linear systems of equations with random right hand sides solved to a relative residual tolerance of 10^{-8} using the conjugate gradient method. Iteration counts and condition number estimates of the preconditioned operator are denoted by `iter` and `cond`, respectively, in the tables.

Selected results are also presented for two variants of the preconditioner. Variant 1 uses a multiplicative coarse correction rather than an additive one; see, e.g., [34, Section 3.2.1]. In this case, the Schwarz method is based on the polynomial

$$P_{v1} = (I - P_0) \left(I - \sum_{i=1}^N P_i \right) \left(\sum_{i=1}^N P_{i\delta} \right) \left(I - \sum_{i=1}^N P_i \right) (I - P_0).$$

Comparing P_{v1} with P_{hyb} , we see that the coarse correction is now applied in a first and final step. In practice, however, it is only necessary to apply the coarse correction once for each iteration after an initialization step. Variant 2 is identical to Variant 1 with the exception that $P_{i\delta}$ in the expression above for P_{v1} is replaced by

$$P_{iw\delta} = R_{i\delta}^T \tilde{P}_{iw\delta} \text{ with } \tilde{P}_{iw\delta} \text{ defined by } \tilde{a}_{id}(\tilde{P}_{iw\delta} \mathbf{u}, \mathbf{v}) = \tilde{a}(\mathbf{u}, R_{id}^T D^{-1} \mathbf{v}) \quad \forall \mathbf{v} \in \mathbf{V}_{i\delta},$$

where D is a diagonal matrix; the value of \mathbf{v} at a node is divided by the number of necklace subdomains to which it belongs. Variant 2 basically scales right hand sides prior to applying local solvers. This results in a nonsymmetric preconditioner, and thus the standard conjugate gradient algorithm can no longer be used. Nevertheless, by using a Krylov method which minimizes the energy of the error, just as conjugate gradients does, we find that the number of iterations can be reduced significantly. A related preconditioning strategy is described in [5, Remark 2.7]. We note that we can prove the same bounds for the Schwarz method based on P_{v1} as for P_{hyb} , but that we do not know how to analyze Variant 2. We also note that the range of these two variants of the original hybrid operator also belongs to the space of discrete saddle-point harmonic functions.

We present results for incompressible elasticity in the final example even though our theory does not apply directly to this case; a more thorough treatment will appear elsewhere. It is no longer possible to eliminate pressure unknowns at the element level, and we augment the coarse space with a constant pressure for each subdomain. Thus, the coarse space dimension increases by the number of subdomains, and the coarse problem is a saddle-point system rather than a positive definite one. Right preconditioned GMRES [30, Section 9.3.2] is used as the Krylov subspace method.

5.1. Example 1. The first example is for a unit cube domain decomposed into 64 smaller cube subdomains as shown in Fig. 5.1. Here we use $Q_2 - P_1$ elements, and include a single layer of elements on either side of subdomain boundaries for the necklace subdomains (see Fig 5.1 right). The Poisson ratio ν is the same in each of the subdomains, and Young's modulus E equals σ in the red (light) subdomains and 1 in the blue (dark) subdomains. We note for $\sigma \neq 1$ that this checkerboard distribution of material properties is not quasi-monotone, cf. [11]. Results with essential boundary conditions, on different subsets of the boundary $\partial\Omega$, are given in Table 5.1.

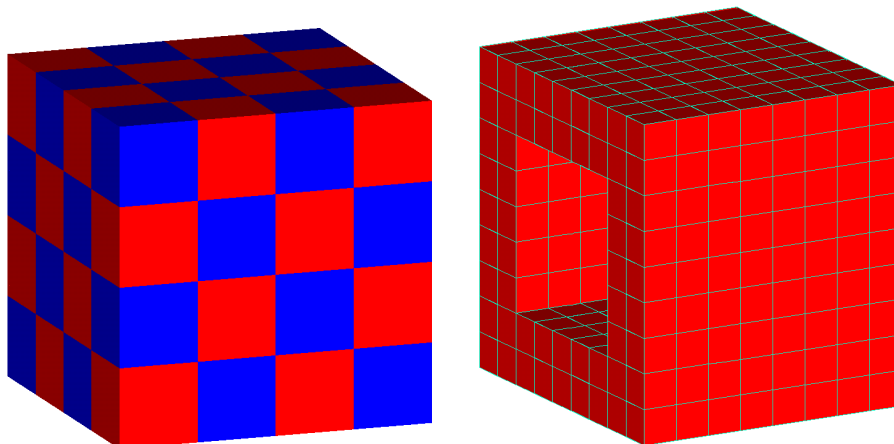


FIG. 5.1. Domain decomposition of cube domain for Example 1 (left) and an example necklace subdomain taken from the left side of the cube and magnified (right).

TABLE 5.1

Example 1 results for $H/h = 7$ and $H/\delta = 7$. The number of unknowns, Poisson ratio, and number of coarse degrees of freedom are denoted by $ndof$, ν , and $ncdof$, respectively.

corners + edges + face bubble for coarse space, $ncdof = 765$												
	all sides constrained, $ndof = 499,125$						left side only constrained, $ndof = 545,832$					
ν	$\sigma = 1$		$\sigma = 100$		$\sigma = 10,000$		$\sigma = 1$		$\sigma = 100$		$\sigma = 10,000$	
	iter	cond	iter	cond	iter	cond	iter	cond	iter	cond	iter	cond
0.3	38	19.6	56	35.3	57	38.0	51	25.4	87	74.0	95	98.3
0.4	42	20.6	59	38.6	61	41.6	53	27.5	93	79.8	100	104
0.49	49	30.5	70	53.3	74	58.2	63	35.7	109	105	115	128
0.499	50	35.3	71	60.9	77	65.7	67	39.3	113	116	121	139
0.4999	52	37.3	70	65.5	77	66.4	68	40.4	115	120	123	147
corners + edges only for coarse space, $ncdof = 621$												
0.3	40	20.3	62	48.9	64	53.4	52	26.8	118	125	131	171
0.4	44	22.9	68	56.8	70	62.8	56	29.2	128	143	141	191
0.49	66	60.7	91	103	104	136	82	63.9	162	232	181	281
0.499	82	113	107	153	123	205	101	110	181	284	211	471
0.4999	88	132	113	186	126	183	108	124	190	313	217	432

The results in Table 5.1 exhibit similar trends whether all six sides of the cube are constrained or just one. For values of ν not too close to the incompressible limit of $1/2$, the coarse spaces with and without an independent degree of freedom for each subdomain face lead to very similar results. In contrast, results are insensitive to changes in ν near $1/2$ only for the coarse space that includes independent face degrees of freedom. We also see that the results are fairly insensitive to jumps in the material property σ as predicted by theory.

5.2. Example 2. We now fix $\nu = 0.3$ in the previous example, and vary the ratio H/h while keeping the overlap ratio $H/\delta = 4$ fixed. In addition, $Q_1 - P_0$ elements are used instead of $Q_2 - P_1$ elements in order to allow us to confirm a condition number estimate for larger values of H/h . Results are shown in Table 5.2 for the coarse space based on corners and edges only (c+e) and the richer coarse space of [10] based on corners, edges, and faces (c+e+f). A logarithmic plot of these results in Figure 5.2 suggests for the c+e coarse space that the exponent p of the factor $(1 + \log(H/h))^p$

TABLE 5.2

Example 2 results for $\nu = 0.3$, $H/\delta = 4$, and left side only constrained.

H/h	ndof	$\sigma = 1$				$\sigma = 100$			
		c+e+f		c+e		c+e+f		c+e	
		iter	cond	iter	cond	iter	cond	iter	cond
4	13,872	31	13.5	37	15.9	35	15.0	71	55.0
8	104,544	39	17.6	43	19.9	45	19.5	88	72.2
12	345,744	42	19.9	45	22.3	49	22.1	91	84.2
16	811,200	44	21.5	47	24.0	51	23.9	95	93.1
20	1,574,640	46	22.7	49	25.4	53	25.2	100	100
24	2,709,792	47	23.7	50	26.4	55	26.2	104	106

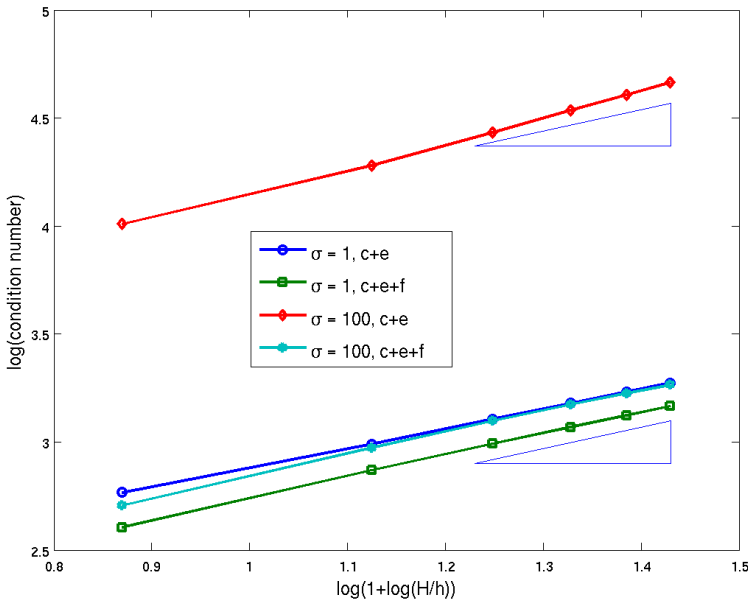


FIG. 5.2. Logarithmic plot of Table 5.2 data. The two triangles in the figure have unit slopes.

in the condition number estimate is no greater than 2 for both $\sigma = 1$ and $\sigma = 100$. Indeed, for $\sigma = 1$ we observe $p \approx 1$ and p is only slightly greater than 1 for $\sigma = 100$. These results suggest it may be possible to reduce p from 2 to 1 in our current theory, at least, for quasi-monotone coefficient distributions. Consistent with the theory for the unreduced coarse space [10], the exponent p appears to be bounded above by 1 for c+e+f for both values of σ ; we note that a factor in the bound in [10] has recently been improved from $(1 + \log(H/h))^2$ to $(1 + \log(H/h))$.

5.3. Example 3. The next example is used to demonstrate the scalability of our algorithm with respect to the number of subdomains. Here again, we consider a unit cube decomposed into smaller cubic subdomains having $H/h = 7$ and $H/\delta = 7$, but now both E and ν are constant. The results in Table 5.3 show that only the coarse space with face degrees of freedom leads to a scalable algorithm as ν approaches $1/2$. Both coarse spaces, however, are scalable for values of ν not too close to $1/2$.

TABLE 5.3

Example 3 results for N subdomains with $H/h = 7$ and $H/\delta = 7$. The coarse space based on corners and edges only is designated by $c+e$, while $c+e+b$ denotes the same coarse space augmented with a single degree of freedom for each subdomain face. All six sides of the domain are constrained.

N	ndof	Poisson ratio $\nu = 0.3$				Poisson ratio $\nu = 0.4999$			
		c+e+b		c+e		c+e+b		c+e	
		iter	cond	iter	cond	iter	cond	iter	cond
8	59,049	28	12.7	28	14.8	50	45.6	62	227
27	206,763	35	17.0	37	19.0	51	37.7	77	106
64	499,125	38	19.6	40	20.3	52	37.3	88	132
125	985,527	42	21.1	41	21.7	52	38.3	94	148
216	1,715,361	43	22.1	44	22.6	53	39.1	98	158
343	2,738,019	45	22.9	46	23.3	53	39.6	100	162
512	4,102,893	46	23.5	46	23.8	53	39.9	102	169

TABLE 5.4

Example 4 results for 64 subdomains with $H/h = 12$. The left side of the domain is fixed and there are 1,196,712 unknowns. The coarse space includes corners, edges, and one degree of freedom for each subdomain face.

H/δ	$\nu = 0.3$		$\nu = 0.499$	
	iter	cond	iter	cond
3	46	23.0	62	35.5
4	49	25.4	65	38.7
6	54	28.2	73	44.0
12	61	33.0	120	136

5.4. Example 4. In the fourth example, we fix $H/h = 12$ and vary H/δ for a unit cube domain decomposed into 64 smaller cube subdomains. We see a much stronger dependence on the overlap parameter H/δ for values of ν near $1/2$ as predicted by theory.

5.5. Example 5. Here we consider the two meshes and mesh decompositions shown in Figs. 5.3 and 5.4. The material properties are constant throughout the structure in Fig. 5.3, while those for the structure in Fig. 5.4 vary as described in the caption. Notice for the decomposition of Mesh 2 that material properties are not constant in each subdomain. Although our theory does not cover this important case, the algorithm appears to perform well for this problem. Nor does the theory apply to the Mesh 1 problem with constant material properties because it has irregular-shaped subdomains. We also note that the theory does not apply for meshes of $Q_1 - P_0$ elements if ν is close to $1/2$ because this element is not inf-sup stable. Nevertheless, we observe satisfactory performance of our algorithm in this case as well. Variants 1 and 2 of the preconditioner both lead to noticeable reductions in iteration counts over all values of Poisson ratio for meshes of $Q_2 - P_1$ elements. The same does not necessarily hold for meshes of $Q_1 - P_0$ elements near the incompressible limit. The mesh decompositions for this example were obtained using a tool based on the graph partitioning program Chaco [14].

5.6. Example 6. With reference to Examples 1 and 3, we now investigate the scalability of our method for the incompressible case of $\nu = 1/2$. In contrast to the previous examples, we do not eliminate displacement and pressure unknowns in subdomain interiors. Moreover, we use standard overlapping subdomains, as in [10], rather than the necklace subdomains. As was true for compressible and almost incompressible cases, it is apparent in Table 5.6 that the method has very good scalability

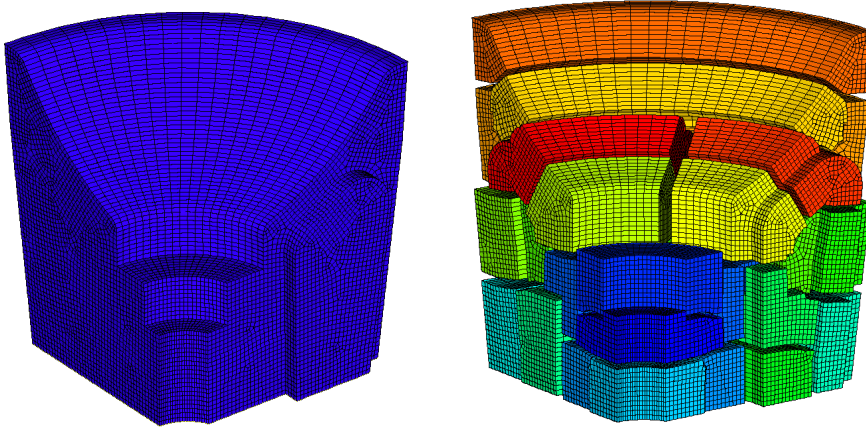


FIG. 5.3. Mesh 1 for Example 5 and decomposition into 20 subdomains. Young's modulus and Poisson ratio are constant with $E = 10e6$ and ν given in Table 5.5. All three degrees of freedom of nodes at the bottom of the mesh are fixed.

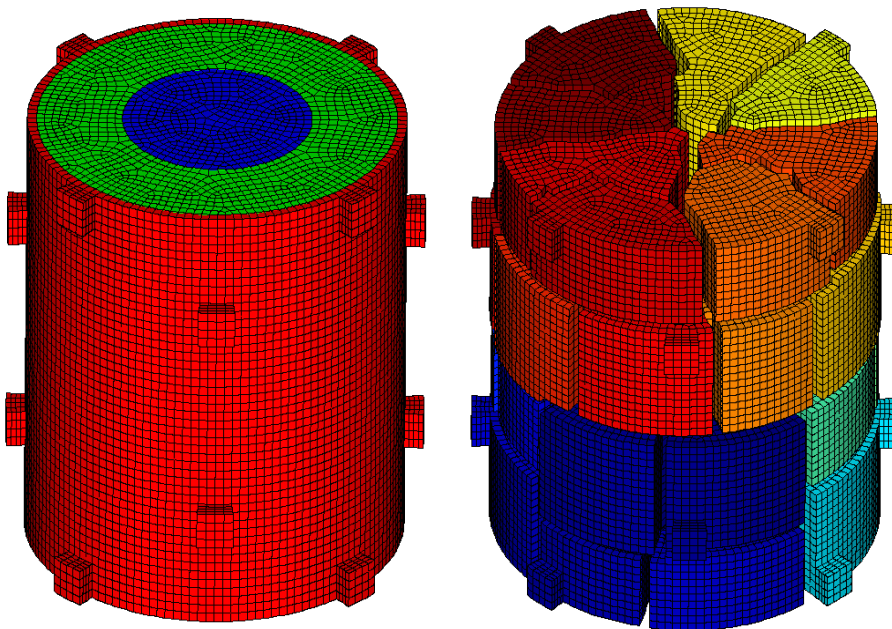


FIG. 5.4. Mesh 2 for Example 5 and decomposition into 40 subdomains. The material properties in the inner(1), middle(2), and outer(3) cylindrical regions (see left figure) are $(E_1, E_2, E_3) = (30e6, 15e6, 10e6)$ and $(\nu_1, \nu_2, \nu_3) = (0.3, \nu, 0.33)$, where ν is given in Table 5.5. All three degrees of freedom of nodes at the bottom of the mesh are fixed.

TABLE 5.5

Example 5 results for meshes and decompositions shown in Figs. 5.3 and 5.4. M^{-1} denotes the subject preconditioner of this study, while $M_{v_1}^{-1}$ and $M_{v_2}^{-1}$ are the two variants described at the beginning of this section. The coarse space includes the additional degree of freedom for each subdomain face, and two layers of elements on either side of subdomain boundaries are used for the necklace (overlap) subdomains.

Mesh 1 results for 20 subdomains										
	$Q_2 - P_1$, $ndof = 1,196,712$					$Q_1 - P_0$, $ndof = 155,106$				
	M^{-1}		$M_{v_1}^{-1}$		$M_{v_2}^{-1}$	M^{-1}		$M_{v_1}^{-1}$		$M_{v_2}^{-1}$
ν	iter	cond	iter	cond	iter	iter	cond	iter	cond	iter
0.3	87	159	79	137	48	87	153	73	120	51
0.4	97	199	88	171	57	96	196	82	153	59
0.49	143	520	137	444	92	156	581	136	437	105
0.499	175	867	165	711	112	206	1.13e3	184	821	159
0.4999	182	954	175	778	117	228	1.32e3	200	929	287
Mesh 2 results for 40 subdomains										
	$Q_2 - P_1$, $ndof = 2,046,528$					$Q_1 - P_0$, $ndof = 261,888$				
0.3	59	29.8	42	16.9	23	50	21.9	36	13.2	21
0.4	61	32.4	47	21.6	26	53	24.2	40	16.8	24
0.49	77	55.6	61	41.8	36	67	41.7	53	31.8	34
0.499	84	66.2	67	49.9	39	75	48.3	59	38.1	41
0.4999	85	69.8	69	52.8	40	88	55.5	78	51.5	54

TABLE 5.6

Incompressible elasticity results (iterations) for structured mesh decompositions with $H/h = 7$ and $H/\delta = 7$. All six faces of the cube domain are constrained, and the coarse space includes the additional degree of freedom for each subdomain face.

N	$ndof$	$\sigma = 1$			$\sigma = 100$		
		M^{-1}	$M_{v_1}^{-1}$	$M_{v_2}^{-1}$	M^{-1}	$M_{v_1}^{-1}$	$M_{v_2}^{-1}$
8	70,025	41	41	25	37	32	23
27	243,807	48	43	33	51	38	30
64	586,933	50	44	35	60	39	34
125	1,157,027	51	45	36	62	40	35
216	2,011,713	52	44	36	64	40	36
343	3,208,615	52	44	36	65	40	37
512	4,805,357	52	44	37	65	40	37

with respect to the number of subdomains. Condition number estimates are not provided in Table 5.6 because GMRES was used rather than conjugate gradients for this example.

REFERENCES

- [1] Manoj Bhardwaj, Garth Reese, Brian Driessen, Kenneth Alvin, and David Day. Salinas - an implicit finite element structural dynamics code developed for massively parallel platforms. In *41st AIAA/ASME/ASCE/AHS/ASC SDM April 3-6, 2000/Atlanta, GA*, AIAA 2000-1651, 2000.
- [2] James H. Bramble, Joseph E. Pasciak, and Alfred H. Schatz. The construction of preconditioners for elliptic problems by substructuring. IV. *Math. Comp.*, 53(187):1–24, 1989.
- [3] Susanne C. Brenner and Ridgway Scott. *The Mathematical Theory of Finite Element Methods*. Springer-Verlag, Berlin, Heidelberg, New York, 2008. Third edition.
- [4] Franco Brezzi and Michel Fortin. *Mixed and Hybrid Finite Element Methods*. Springer-Verlag, 1991.
- [5] Xiao-Chuan Cai and Marcus Sarkis. Timely Communication: A restricted additive Schwarz preconditioner for general sparse linear systems. *SIAM J. Sci. Comput.*, 21(2):792–797, 1999.
- [6] Clark R. Dohrmann. A preconditioner for substructuring based on constrained energy mini-

- mization. *SIAM J. Sci. Comput.*, 25(1):246–258, 2003.
- [7] Clark R. Dohrmann. Preconditioning of saddle point systems by substructuring and a penalty approach. In David E. Keyes and Olof B. Widlund, editors, *Domain Decomposition Methods in Sciences and Engineering XVI*, number 55 in Lecture Notes in Computational Science and Engineering, pages 53–64. Springer-Verlag, 2006. Proceedings of the 16th International Conference on Domain Decomposition Methods, held in New York City, January 11–15, 2005.
- [8] Clark R. Dohrmann, Axel Klawonn, and Olof B. Widlund. A family of energy minimizing coarse spaces for overlapping Schwarz preconditioners. In Ulrich Langer, Marco Discacciati, David Keyes, Olof Widlund, and Walter Zulehner, editors, *Proceedings of the 17th International Conference on Domain Decomposition Methods in Science and Engineering, held in Strobl, Austria, July 3-7, 2006*, number 60 in Springer-Verlag, Lecture Notes in Computational Science and Engineering, pages 247–254, 2007.
- [9] Clark R. Dohrmann, Axel Klawonn, and Olof B. Widlund. Domain decomposition for less regular subdomains: Overlapping Schwarz in two dimensions. *SIAM J. Numer. Anal.*, 46(4):2153–2168, 2008.
- [10] Clark R. Dohrmann and Olof B. Widlund. An overlapping Schwarz algorithm for almost incompressible elasticity. Technical Report TR2008-912, Courant Institute of Mathematical Sciences, May 2008. URL: <http://cs.nyu.edu/csweb/Research/TechReports/TR2008-912/TR2008-912.pdf>.
- [11] Maksymilian Dryja, Marcus V. Sarkis, and Olof B. Widlund. Multilevel Schwarz methods for elliptic problems with discontinuous coefficients in three dimensions. *Numer. Math.*, 72:313–348, 1996.
- [12] Maksymilian Dryja, Barry F. Smith, and Olof B. Widlund. Schwarz analysis of iterative substructuring algorithms for elliptic problems in three dimensions. *SIAM J. Numer. Anal.*, 31(6):1662–1694, 1994.
- [13] Paulo Goldfeld, Luca F. Pavarino, and Olof B. Widlund. Balancing Neumann-Neumann preconditioners for mixed approximations of heterogeneous problems in linear elasticity. *Numer. Math.*, 95(2):283–324, 2003.
- [14] Bruce Hendrickson and Robert Leland. The Chaco User’s Guide: Version 2.0. Technical Report SAND94-2692, Sandia National Laboratories, 1994.
- [15] Thomas J.R. Hughes. *The Finite Element Method: Linear Static and Dynamic Finite Element Analysis*. Prentice-Hall, Inc., Englewood Cliffs, New Jersey, 1987.
- [16] Axel Klawonn and Luca F. Pavarino. Overlapping Schwarz methods for mixed linear elasticity and Stokes problems. *Comput. Methods Appl. Mech. Engrg.*, 165:233–245, 1998.
- [17] Axel Klawonn and Luca F. Pavarino. A comparison of overlapping Schwarz methods and block preconditioners for saddle point problems. *Numer. Lin. Alg. Appl.*, 7:1–25, 2000.
- [18] Axel Klawonn and Oliver Rheinbach. Robust FETI-DP methods for heterogeneous three dimensional linear elasticity problems. *Comput. Methods Appl. Mech. Engrg.*, 196(8):1400–1414, 2007.
- [19] Axel Klawonn, Oliver Rheinbach, and Olof B. Widlund. An analysis of a FETI-DP algorithm on irregular subdomains in the plane. *SIAM J. Numer. Anal.*, 46(5):2484–2504, 2008.
- [20] Axel Klawonn and Olof B. Widlund. Dual-Primal FETI methods for linear elasticity. *Comm. Pure Appl. Math.*, 59(11):1523–1572, November 2006.
- [21] Jing Li. A dual-primal FETI method for incompressible Stokes equations. *Numer. Math.*, 102:257–275, 2005.
- [22] Jing Li and Olof B. Widlund. BDDC algorithms for incompressible Stokes equations. *SIAM J. Numer. Anal.*, 44(6):2432–2455, 2006.
- [23] Jan Mandel. Iterative solvers by substructuring for the p-version finite element method. *Comput. Methods Appl. Mech. Engrg.*, 80:117–128, 1990.
- [24] Jan Mandel. Hybrid domain decomposition with unstructured subdomains. In Jan Mandel, Charbel Farhat, and Xiao-Chuan Cai, editors, *Domain Decomposition Methods in Science and Engineering. Sixth International Conference of Domain Decomposition*, pages 103–112. AMS, Contemporary Mathematics 157, 1994. Como, Italy, June 15–19, 1992.
- [25] Jan Mandel and Marian Brezina. Balancing domain decomposition for problems with large jumps in coefficients. *Math. Comp.*, 65(216):1387–1401, 1996.
- [26] Jindřich Nečas. *Les méthodes directes en théorie des équations elliptiques*. Academia, Prague, 1967.
- [27] Luca F. Pavarino and Olof B. Widlund. Iterative substructuring methods for spectral element discretizations of elliptic systems. I. Compressible linear elasticity. *SIAM J. Numer. Anal.*, 37(2):353–374, 2000.
- [28] Rodrigo R. Paz, Norberto M. Nigro, and Mario A. Storti. On the efficiency and quality of

- numerical solutions in CFD problems using the interface strip preconditioner for domain decomposition methods. *Internat. J. Numer. Methods Fluids*, 52(1):89–118, 2006.
- [29] Alfio Quarteroni, Marzio Sala, and Alberto Valli. An interface-strip domain decomposition preconditioner. *SIAM J. Sci. Comput.*, 28(2):498–516, 2006.
 - [30] Yousef Saad. *Iterative Methods for Sparse Linear Systems*. SIAM, Philadelphia, Pennsylvania, 2003.
 - [31] Barry F. Smith. *Domain Decomposition Algorithms for the Partial Differential Equations of Linear Elasticity*. PhD thesis, Courant Institute of Mathematical Sciences, September 1990. Tech. Rep. 517, Department of Computer Science, Courant Institute.
 - [32] Barry F. Smith. A domain decomposition algorithm for elliptic problems in three dimensions. *Numer. Math.*, 60(2):219–234, 1991.
 - [33] Barry F. Smith. An optimal domain decomposition preconditioner for the finite element solution of linear elasticity problems. *SIAM J. Sci. Stat. Comput.*, 13(1):364–378, January 1992.
 - [34] Barry F. Smith, Petter Bjørstad, and William Gropp. *Domain Decomposition: Parallel Multilevel Methods for Elliptic Partial Differential Equations*. Cambridge University Press, New York, 1996.
 - [35] Andrea Toselli and Olof Widlund. *Domain Decomposition Methods - Algorithms and Theory*, volume 34 of *Springer Series in Computational Mathematics*. Springer-Verlag, Berlin Heidelberg New York, 2005.